

BCL::MP-Fold: membrane protein structure prediction guided by EPR restraints

Short title: EPR guided membrane protein fold prediction

Keywords: de novo folding; proteins; membrane proteins; limited experimental data; protein structure determination

Axel W. Fischer^{1,2,3}, Nathan S. Alexander^{1,2,3}, Nils Woetzel^{1,2}, Mert Karakas², Brian E. Weiner^{1,2}, Jens Meiler^{1,2}.

1. Department of Chemistry, Vanderbilt University, Nashville, TN 37232, USA
2. Center for Structural Biology, Vanderbilt University, Nashville, TN 37232, USA
3. Contributed equally to this article

Contact

Jens Meiler, Ph.D.

Associate Professor

Vanderbilt University

Departments of Chemistry and Pharmacology

Center for Structural Biology

465 21st Ave South

BIOSCI/MRBIII, Room 5144B

Nashville, TN 37232-8725

USA

E-Mail: jens.meiler@vanderbilt.edu

URL : www.meilerlab.org

Phone: +1 (615) 936-5662

Phone: +1 (615) 936-2209 (secretary)

This article has been accepted for publication and undergone full peer review but has not been through the copyediting, typesetting, pagination and proofreading process which may lead to differences between this version and the Version of Record. Please cite this article as an 'Accepted Article', doi: 10.1002/prot.24801

© 2015 Wiley Periodicals, Inc.

Received: Nov 01, 2014; Revised: Mar 11, 2015; Accepted: Mar 20, 2015

Abstract

For many membrane proteins, the determination of their topology remains a challenge for methods like X-ray crystallography and nuclear magnetic resonance (NMR) spectroscopy. Electron paramagnetic resonance (EPR) spectroscopy has evolved as an alternative technique to study structure and dynamics of membrane proteins. The present study demonstrates the feasibility of membrane protein topology determination using limited EPR distance and accessibility measurements. The BCL::MP-Fold (BioChemical Library membrane protein fold) algorithm assembles secondary structure elements (SSEs) in the membrane using a Monte Carlo Metropolis (MCM) approach. Sampled models are evaluated using knowledge-based potential functions and agreement with the EPR data and a knowledge-based energy function. Twenty-nine membrane proteins of up to 696 residues are used to test the algorithm. The RMSD100 value of the most accurate model is better than 8Å for twenty-seven, better than 6Å for twenty-two and better than 4Å for fifteen out of twenty-nine proteins, demonstrating the algorithm's ability to sample the native topology. The average enrichment could be improved from 1.3 to 2.5, showing the improved discrimination power by using EPR data.

Introduction

Membrane protein structure determination continues to be a challenge. About 22% of proteins are membrane proteins and an estimated 60% of pharmaceutical therapies target membrane proteins¹. However, only 2.5% of the proteins deposited in the Protein Data Bank are classified as membrane proteins^{2,3}. Protein structures are typically determined to atomic detail using X-ray crystallography or NMR spectroscopy. However membrane proteins provide challenges for both techniques⁴. It is difficult to obtain quantities of purified membrane proteins sufficient for both,

X-ray crystallography and NMR. The two-dimensional nature of the membrane complicates crystallization in a three-dimensional crystal lattice. In order to obtain crystals, the target protein is often subjected to non-native-like environments and/or modifications such as stabilizing sequence mutations^{5,6}. Additional problems may evolve from posttranslational modification such as phosphorylation⁷. Many membrane proteins continue to be too large for structure determination by NMR spectroscopy⁸. Even if the target itself is not too large, the membrane mimic adds significant additional mass to the system⁹. Despite wonderful successes in determining the structure of high-profile targets, it is critical that the structural features observed with one technique are confirmed with an orthogonal technique¹⁰.

EPR spectroscopy in conjunction with site-directed-spin-labeling (SDSL) provides such an orthogonal technique for probing structural aspects of membrane proteins¹¹⁻¹³. Advantages of EPR spectroscopy include that the protein can be studied in a native-like environment and that only a relatively small sample amount is required. In addition, EPR spectroscopy can be used to study large proteins. Although EPR is a versatile tool for probing membrane protein structure, it has its own challenges: at least one unpaired electron (spin label) needs to be introduced into the protein. Typically, this requires mutation of all cysteine residues to either alanine or serine, introduction of one or two cysteines at the desired labeling sites, coupling to the thiol-specific nitroxide spin label MTSSL, and functional characterization of the protein. As a result, datasets from EPR spectroscopy are sparse containing only a fraction of measurements per residue in the target protein. EPR is not a high-throughput technique.

EPR provides two categories of structural information important to membrane protein topology: First, EPR can provide information about the local environment of the spin label¹⁴⁻¹⁶. The accessibility of the spin label to oxygen probe molecules indicates the degree of burial of the spin

label within the protein in the trans-membrane region. Accessibility measurements are typically performed in a sequence scanning fashion. This provides an accessibility profile over a large portion of the sequence^{17,18}. The accessibility profile tracks the periodicity of SSEs as individual measurements rise and fall according to the periodic exposure and burial of residues. The exposed face of a SSE can be determined¹⁹, a task that is difficult within the hydrophobic environment of the membrane. Secondly, when two spin labels are introduced, EPR can measure inter-spin label distances, routinely of up to 60Å through the DEER experiment^{20,21}. EPR distance measurements have been demonstrated on several large membrane proteins including MsbA²², rhodopsin²³, and LeuT²⁴. Given the sparseness of data, EPR has been frequently used to probe different structural states of proteins^{25,26}. Changes in distances and accessibilities track regions of the protein that move when converting from one state into another. Such investigations rely upon an already determined experimental structure to define the protein topology and provide a scaffold to map changes observed via EPR spectroscopy.

One critical limitation for *de novo* protein structure prediction from EPR data is that measurements relate to the tip of the spin label side chain where the unpaired electron is located while information of the placement of backbone atoms is needed to define the protein fold. For distance measurements, this introduces an uncertainty in relating the distance measured between the two spin labels to a distance between points in the backbone of the protein. This uncertainty, defined as the difference between the distance between the spin labels and the distance between the corresponding C_β atoms is up to 12Å^{27,28}. To address this uncertainty we previously introduced a cone model which provides a knowledge-based probability distribution for the C_β atom distance given an EPR-measured spin label distance^{27,29}. Using the cone model, just 25 or even 8 EPR measured distances for T4-lysozyme, enabled Rosetta to provide models matching

the experimentally determined structure to atomic detail including backbone and side-chain placement²⁷. Further success was reported by Yang³⁰, who successfully determined the tertiary structure of a homo-dimer by using inter-chain restraints determined from NMR and EPR experiments. These studies demonstrate that *de novo* prediction methods can supplement EPR data sufficiently to allow structure elucidation of a protein.

De novo membrane protein structure prediction was demonstrated with Rosetta using twelve proteins with multiple transmembrane spanning helices³¹. The method was generally successful for the membrane topology for small proteins up to 278 residues. The results of the study suggest that sampling of large membrane topologies requires methods that directly sample structural contacts between sequence distance regions of the protein³².

For this purpose we developed an algorithm that assembles protein topologies from SSEs termed BCL::Fold³³. The omission of loop regions in the initial protein folding simulation allows sampling of structural contacts between regions distant in sequence and thereby rapidly enumerates all likely protein topologies. A knowledge-based potential guides the algorithm towards physically realistic topologies. The algorithm is particularly applicable for the determination of membrane protein topologies as trans-membrane spans are dominated by regularly ordered SSEs³⁴. Loop regions and amino acid side chains can be added in later stages of modeling structure. The algorithm was tested in conjunction with medium resolution density maps³⁵ achieving models accurate at atomic detail in favorable cases³⁶. The algorithm was also tested in conjunction with sparse NMR data³⁷.

The present study combines EPR distance and accessibility restraints with the BCL::Fold SSE assembly methodology for the prediction of membrane protein topologies. In a first step, we

introduce scores specific to EPR distances and accessibilities and demonstrate their ability to enrich for accurate models. In a second step, we assemble twenty-three monomeric and six multimeric membrane proteins guided by EPR distance and accessibility restraints. The results show that the inclusion of protein specific structural information improves the frequency with which accurate models are sampled and greatly improves the discrimination of incorrect models.

Materials and Methods

Compilation of the benchmark set

Twenty-nine membrane proteins of known structure were used to demonstrate the ability of EPR specific scores to improve sampling during protein structure prediction as well as selecting the most accurate models. The proteins for the benchmark were chosen to cover a wide range of sequence length, number of SSEs and percentage of residues within SSEs (Table I). Twenty-three of the proteins are monomers ranging in size from 91 to 568 residues. One protein (2L35) has two chains, with the second chain being a single transmembrane span. The remaining five proteins are symmetric multimeric proteins of two or three subunits containing up to 696 residues. 5000 independent structure prediction trajectories are conducted for each protein without restraints, with distance restraints only, with accessibility restraints only, and with distance and accessibility restraints. In order to achieve results that are independent of one specific spin labelling pattern, ten different restraint sets are used for each protein. Those trajectories are conducted with SSEs predicted from sequence and, to test the influence of incorrectly predicted secondary structure, with the SSEs obtained from the experimentally determined structure. In addition, rhodopsin (protein data bank entry 1GZM) was added to the

benchmark set to demonstrate the algorithms' ability to work with experimentally determined restraints.

Simulation of EPR restraints

For 1GZM EPR distance restraints were available²³, while for the other proteins EPR distance and accessibility restraints were simulated to obtain datasets for each of the twenty-nine proteins. Accessibility restraints were simulated by calculating the neighbor vector value³⁸ for residues within SSEs of each protein. Unlike the neighbor count approximation of solvent accessible surface area (SASA), the neighbor vector approach takes the relative placement of the neighbors with respect to the vector from the C_{α} atom to the C_{β} atom into account. It thereby becomes a more accurate predictor of SASA³⁸. The resulting exposure value for each residue was considered an oxygen accessibility measurement. One restraint per two residues within the trans-membrane segment of each SSE was simulated.

Distance restraints were simulated using a restraint selection algorithm³⁹ which distributes measurements across all SSEs. It also favors measurements between residues that are far apart in sequence. One restraint was generated per five residues within the trans-membrane segment of an SSE, if not indicated otherwise. Distances are calculated between the C_{β} atoms; for glycine, the $H_{\alpha 2}$ atom is used. To simulate a likely distance observed in an actual EPR experiment, the distance is adjusted by an amount selected randomly from the probability distribution of observing a given difference between the spin-spin distance (D_{SL}) and the back bone distance (D_{BB})²⁸. In order to reduce the possibility of bias arising from restraint selection and spin labelling patterns, ten independent restraint sets were generated. For the five symmetric

multimeric proteins, the same protocol was used, but only distance restraints between the same residues in the different subunits were considered.

Translating EPR accessibilities into structural restraints

EPR accessibility measurements are typically made in a sequence scanning fashion over a portion of the target protein. While each individual accessibility measurement is difficult to interpret, the pattern of accessibilities over a stretch of amino acids within an SSE indicates reliably which phase of the SSE is exposed to solvent/membrane versus buried in the protein core. We found accessibility restraints to have a limited impact on structure prediction for soluble proteins²⁷. We concluded that this is the case as knowledge-based potentials on their own can distinguish the polar phase of an SSE that is exposed to an aqueous solvent from a hydrophobic phase buried in the protein core. However, we also hypothesized that the situation will be different for membrane proteins where it would be harder to distinguish the membrane-exposed from the buried phase of an α -helix as both of these tend to be apolar.

Our approach for developing an EPR accessibility score takes advantage of the regular geometry within the SSE: The exposure moment of a window of amino acids is defined as $E_w = \sum_{n=1}^N e_n s_n$, where N is the number of residues in the window, e_n is the exposure value of residue n , and s_n is the normalized vector from the C_α atom to the C_β atom of residue n . This equation was inspired by the hydrophobic moment as previously defined⁴⁰. The exposure moment calculated from solvent accessible surface area SASA has been previously shown to approximate the moment calculated from EPR accessibility measurements¹⁹.

During *de novo* protein structure prediction, the protein is represented only by its backbone atoms hampering calculation of SASA. Further, calculation of SASA from an atomic-detail

model would be computationally prohibitive for a rapid scoring function in *de novo* protein structure prediction. Therefore, the neighbor vector approximation for SASA is used³⁸. The exposure moment is calculated for overlapping windows of length seven for α -helices and four for β -strands. The score is computed as $S_{orient} = -\frac{1}{2} \cos(\theta)$ where θ is the torsion angle between the exposure moments. This procedure assigns a score of -1 is given if $\theta = 0^\circ$ and a score of 0 if $\theta = 180^\circ$ (Figure 1).

Figure 1

It has previously been demonstrated that the burial of sequence segments relative to other segments can be determined from the average accessibility values measured for that stretch of sequence⁴¹. To capture this information, the magnitude of the exposure moment for overlapping residue windows is determined from the model structure and from the measured accessibility. The Pearson correlation is then calculated between the rank order magnitudes of the structural versus experimental moments. This gives a value between -1 which indicates the structural and exposure magnitudes are oppositely ordered, and 1, which means the structural and exposure magnitudes are ordered equivalently. The score S_{magn} is obtained by negating the resulting Pearson correlation value so that matching ordering will get a negative score and be considered favorable.

Translating EPR distances into structural restraints

The motion-on-a-cone model²⁷ yields a predicted distribution for the difference between D_{SL} and D_{BB} . This distribution was converted into a knowledge-based potential function which is used to score the agreement of models with experimentally determined EPR distance restraints²⁸. This score spans a range of $D_{SL} - D_{BB}$ between $\pm 12\text{\AA}$. D_{SL} is the EPR measured distance between the

two spin labels; D_{BB} is the distance between the corresponding C_{β} or $H_{\alpha 2}$ atoms on the residues of interest; $D_{SL} - D_{BB}$ is the difference between these two distances (Figure 1).

In addition, we found it beneficial to add an attractive potential on either side of the range spanned by the scoring function to provide an incentive for the MCM minimization to bring structures within the defined range of the scoring function. These attractive potentials use a cosine function to transition between a most unfavorable score of 0 and a most favorable score of -1. The attractive potential is positive for $30\text{\AA} \geq |D_{SL} - D_{BB}| \geq 12\text{\AA}$. It levels to 0 when the difference between D_{BB} and D_{SL} approaches 12\AA .

Summary of the folding protocol

The protein structure prediction protocol (Figure 2) is based on the protocol of BCL::Fold for soluble proteins³³. The method assembles SSEs in the three-dimensional space, drawing from a pool of predicted SSEs. A Monte Carlo energy minimization with the Metropolis criteria is used to search for models with favorable energies. Models are scored after each Monte Carlo step using knowledge-based potentials describing optimal SSE packing, radius of gyration, amino acid exposure, and amino acid pairing, loop closure geometry, secondary structure length and content, and penalties for clashes⁴².

The algorithm was adapted for membrane protein folding by altering the amino acid exposure potential according to an implicit membrane environment³⁴. Additional scores are used which favor orthogonal placement of SSEs relative to the membrane (SSE_{align}) and penalizing models with loops going through the membrane (MP_{Top}). All moves introduced for soluble proteins are used³³. In addition, we include perturbations³³ that optimize the placement of the protein in the

membrane such as translation of individual SSEs in the membrane as well as rigid body translation and rotation of the entire protein.

Figure 2

The assembly of the protein structure is broken down into five stages of sampling with large structural perturbation moves that can alter the topology of the protein. Each of the five stages lasts for a maximum of 2000 Monte Carlo steps. If an energetically improved structure has not been generated within the previous 400 Monte Carlo steps, the minimization for that stage will cease. Over the course of the five assembly stages, the weight of clashing penalties in the total score is ramped as 0, 125, 250, 375, and 500.

Following the five stages of protein assembly, a structural refinement stage takes place. This stage lasts for a maximum of 2000 Monte Carlo steps and will terminate sooner if an energetically improved model is not sampled within the previous 400 steps. The refinement stage consists of small structural perturbations, which will not drastically alter the topology of the protein model.

After 5000 models have been generated for each protein, the models are filtered according to EPR distance score. The top 10% or 500 models resulting from the structure prediction protocol are selected for a second round of energy minimization. The second round occurs as described above, the only difference being that the minimization uses the SSE placements of a given protein as a starting point. For each starting structure, 10 models are created, resulting in 5000 models. This boot strapping approach which re-optimizes structures that are in good agreement with the EPR restraints and with the knowledge-based potential was beneficial when combining BCL::MP-Fold with limited NMR data and is not applied when no experimental data are used³⁷.

Summary of the benchmark setup

To test the influence of EPR restraints, each protein besides 1GZM was folded in the absence of restraints, with just distance restraints, with just accessibility restraints, and with distance and accessibility restraints. To test the influence of secondary structure prediction accuracy (see methods section), the experiment was repeated with optimal secondary structure elements derived from the experimentally determined structure. 1GZM was only folded without restraints and with the experimentally determined distance restraints. 5000 models were created for each of the benchmark proteins in independent MCM folding trajectories. EPR distance and accessibility scores are used during the five assembly and one refinement stages of structure prediction protocol. The EPR distance scores have a weight of 40 during all assembly and refinement stages using either pool.

Structure prediction protocol

For each protein, two sets of SSE pools are generated for use during structure assembly. The first SSE pool consists of the transmembrane spanning helices as predicted by Octopus. The second SSE pool contains elements predicted by Octopus as well as SSEs predicted from sequence by Jufo9D. Using these two SSE pools, the structure prediction protocol is independently conducted twice: a) once using the SSE pool containing predictions from Octopus and Jufo9D (“full pool”) and b) once emphasizing the predictions by Octopus (“Octopus pool”). Emphasis is placed on Octopus predictions by using only the Octopus generated SSE pool during the first two stages of assembly. During last three stages of structure assembly, the SSEs predicted from Jufo9D are added to the pool. This allows for better coverage of SSEs within the structure, since Octopus only predicts transmembrane spanning helices.

EPR specific scores are used during the five assembly and one refinement stages of structure prediction. The EPR distance scores have a weight of 40 over the course of the assembly and refinement stages.

Calculating EPR score enrichments

The enrichment value is used to evaluate how well a scoring function is able to select the most accurate models from a given set of models. The models of a given set S are sorted by their RMSD100 values. The 10% of the models with the lowest RMSD100 values put into the set P (positive) the rest of the models will be put into the set N (negative). The models of S are then also sorted by their assigned scoring value and the 10% of the models with the lowest (most favorable) score are put into the set T . The models, which are in P and in T are the models, which are correctly selected by the scoring function and their number will be referred to as TP (true positives). The number of models, which are in P but not in T are the models which are not selected by scoring function despite being among the most accurate ones. They will be referred to as FN (false negative). The enrichment will then be calculated as $E = \frac{\#TP}{\#P} \cdot \frac{\#P+\#N}{\#P}$. The positive models are in this case considered the 10% of the models with the lowest RMSD100 values. Therefore $\frac{\#P+\#N}{\#P}$ is a constant value of 10.0. No enrichment would be a value of 1.0 and an enrichment value between 0.0 and 1.0 indicates that the score selects against accurate models.

Results

Using EPR specific scores during membrane protein structure prediction improves sampling accuracy

For each protein, the ten models sampled with the best RMSD100⁴³ values are used to determine ability to sample accurate models by taking their RMSD100 value average, μ_{10} . Using the best ten models by RMSD100 provides a more consistent measure of sampling accuracy compared to looking at the single best because of the random nature of the structure prediction protocol. Additionally, the percentages of models with an RMSD100 less than 4Å and less than 8Å, τ_4 and τ_8 , were calculated.

By using EPR distance and accessibility scores, not only is the frequency increased with which higher accuracy models are sampled, but best models achieve an accuracy not sampled in the absence of EPR data (Table III). Across all proteins, μ_{10} is, on average, 6.0Å when EPR distance and accessibility scores are not used. When adding restraints for distances and then both distances and accessibilities, the average μ_{10} value drops to 5.1Å and 5.0Å, respectively (Table III). By only adding EPR accessibility restraints the average μ_{10} over all proteins improves only slightly to 5.8Å. This shows that the accuracy of the models is primarily improved by using EPR distance restraints in the structure prediction process. With the exception of 1KPL and 2XUT, all proteins achieve a μ_{10} value of less than 8.0Å. This indicates the placement of the transmembrane spanning regions follow the experimentally determined structures and the correct fold could be predicted. Figure 3 compares the RMSD100 values of the average of the 1% most accurate models with and without the usage of EPR distance restraints – an average improvement of 0.8Å over the benchmark is observed. The shift to lower RMSD100 values in distributions for selected benchmark proteins is shown in Figure 4. The average τ_4 and τ_8 values improve from 3% and 13%, when folding without EPR restraints, to 6% and 19% when using EPR restraints, respectively.

The six multimeric proteins achieve an average μ_{10} value of 5.0Å when the structure prediction was conducted without using EPR restraints. By using EPR distance and accessibility restraints μ_{10} could be improved to 2.9Å. The τ_4 and τ_8 values could be improved from 13% and 24% to 21% and 41% when using EPR distance and accessibility restraints in the structure prediction process.

Figure 3

EPR accessibility scores are important for improving contact recovery

EPR accessibility scores were previously used in conjunction with the Rosetta protein structure prediction algorithm²⁷. The scores were applied in a benchmark to predict the structures of the small soluble proteins T4-lysozyme and α A-crystallin. The improvement in sampling models that are more accurate was compared between prediction trajectories using an EPR distance score and trajectories using an EPR distance score coupled with an accessibility score. For T4-lysozyme and α A-crystallin, using the accessibility score did not show a significant improvement in the accuracy of models sampled. This was attributed to the simple rule of exposure that is well captured by the knowledge-based potentials: polar residues tend to be exposed to solvent; apolar residues tend to be buried in the core of the protein.

Membrane proteins are subjected to a more complex set of possible environments. Any given residue can reside buried in the core of the protein or exposed to different environments ranging from the membrane center to a transition region to an aqueous solvent. If the protein fold contains a pore, a residue can be solvent-exposed deep in the membrane⁴⁴. Such a complex interplay of environments will not be as easily distinguished by knowledge-based potentials.

Here it has been demonstrated that using EPR accessibility information consistently improves the contact recovery for highest accurate models.

While improvements regarding sampling accuracy and selection of the most accurate models by RMSD100 is mainly achieved by using EPR distance restraints, EPR accessibility restraints help determining the correct rotation state of SSEs and therefore improves the number of recovered contacts (Figure 3). A contact is defined as being between amino acids, which are separated by at least six residues and have a maximum Euclidean distance of 8Å. We are measuring the percentage of the contacts in the experimentally determined protein structure, which could be recovered in the models. In order to be independent of huge deviations occurring when only looking at the best model sampled, we quantify the average contact recovery of the ten models with the highest contact recovery (ϕ_{10}) and the percentage of models which have more than 20% and 40% of the contacts recovered (γ_{20} , γ_{40}).

For folding without EPR restraints, the average ϕ_{10} value over all twenty-three monomeric proteins was 23% while with accessibility restraints it was 31% (Table IV). Using distance restraints additionally to the accessibility restraints ϕ_{10} remains at 31%. This is showing that improvements in contact recovery are mainly achieved by using EPR accessibility restraints in the structure prediction process. The average γ_{20} and γ_{40} over all twenty-nine proteins for structure prediction without EPR restraints were 5% and 3%. By using EPR accessibility restraints, the values could be improved to 12% and 6%, respectively.

For the six multimeric proteins, improvements in contact recovery by the usage of EPR accessibility restraints are observed as ϕ_{10} , γ_{20} and γ_{40} could be increased to 46%, 25%, and 16% from the previous values of 38%, 17% and 14% when performing protein structure prediction

without EPR data. By complementing the accessibility with distance restraints φ_{10} , γ_{20} and γ_{40} can be improved to 50%, 30%, and 16%.

Figure 4

EPR specific scores select for accurate models of membrane proteins

The ability of EPR specific scores to select for accurate models is tested by calculating enrichment values for structure prediction trials of twenty-nine membrane proteins (Table II).

The enrichment of a scoring function indicates how well the score identifies a protein model that is accurate by a good score. It is computed as the cardinality of the intersection $I = HS \cap P$ with P being the set of the accurate models and HS being the set of the 10% of the models with the most favorable score (see Methods for details)⁴². Accurate is defined as the 10% of the models with the lowest RMSD100 when compared to the experimentally determined structure. Therefore, if a score correctly identifies all accurate models as being accurate, a perfect enrichment would give a value of 10.0.

Enrichment values are computed for the protein models created without experimental restraints. For protein structure prediction without EPR data, the average enrichment value for just the knowledge-based potentials over all twenty-nine proteins is 1.3. By using EPR distance and accessibility data, the average enrichment is improved to 2.5. The enrichment for using EPR distance and accessibility restraints ranges from 1.1 to 6.2. In seventeen out of twenty-nine cases, the enrichment is greater than 2.0. In twenty-three out of twenty-nine cases the enrichment could be improved by at least 0.5 (Table II). By using EPR accessibility data only the average enrichment over all proteins is 1.6, showing that improvements regarding the selection of the most accurate models is mainly caused by EPR distance restraints.

The number of restraints determines the significance of improvements in sampling accuracy

For four proteins, the influence of varying numbers of restraints was examined. In addition to the one restraint per five residues within SSEs setup used for all benchmark cases, the tertiary structure of 1OCC, 1PV6, 1PY6, and 1RHZ was predicted using one restraint per ten residues, one restraint per three residues, and one restraint per two residues within SSEs. For 1PY6 the sampling accuracy could be steadily improved with an increasing number of restraints shown by τ_8 values increasing from 15% to 20% to 24% to 28% to 33% (Table S2 and Figure S1) and μ_{10} values improving from 4.4Å to 4.2Å to 3.6Å to 3.5Å to 3.3Å for structure prediction without restraints, one restraint per ten residues, one restraint per five residues, one restraint per three residues and one restraint per two residues. For 1OCC, 1PV6 and 1RHZ a significant improvement in sampling accuracy is observed for using one restraint per three residues instead of one restraint per ten residues within SSEs which is shown by improvements in τ_8 values from 42% to 53%, 8% to 36% and 6% to 22% and in μ_{10} values from 3.2Å to 1.9Å, 5.3Å to 4.3Å and 4.7Å to 3.3Å. Increasing the number of restraints to one per two residues within SSEs fails to further improve the sampling accuracy. We attribute this observation to significant bends in some of the SSEs that are currently not sampled sufficiently dense by BCL::MP-Fold.

Using experimentally obtained EPR distance restraints for rhodopsin

The benchmark was extended to also contain rhodopsin (protein data bank entry 1GZM) for which EPR distance measurements were available²³. While only sixteen EPR distance restraints were available, which amounts to less than one restraint per ten residues within SSEs, the sampling accuracy as well as the enrichment improve significantly. The μ_{10} values improved from 4.9Å for folding without restraints to 4.4Å when using restraints. The enrichment values

could be improved from 0.6 to 1.2 showing that even a small number of restraints improves discrimination of incorrect models.

Discussion

EPR distance and accessibility restraints can aid the prediction of membrane protein structure. For this purpose, EPR specific scores were coupled with the protein structure prediction method BCL::MP-Fold. BCL::MP-Fold assembles predicted SSEs in space without explicitly modeling the SSE connecting loop regions. This allows for rapid sampling of complex topology that is not easily achieved when an intact protein backbone must be maintained. By adding EPR specific scores to the knowledge-based scoring function, sampling of accurate structures is increased. Additionally the selection of the most accurate models could be improved significantly.

However it has to be clearly stated that – with the exception of bovine rhodopsin (1GZM) – all EPR restraints used in this study were simulated using the cone-model. Therefore, the relevance of our findings depends on how well the cone-model describes the nature of experimental DEER measurements and in particular the mobility of the spin label.

EPR distance scores improve the accuracy of topologies predicted for membrane proteins

EPR distance measurements are associated with large uncertainties in relating the measured spin label – spin label distance into backbone distances. In spite of this, EPR distance measurements provide important data on membrane protein structures^{22–24,45}. In the present study, it has been shown that EPR distance data can significantly increase the frequency with which the correct topology of a membrane protein is sampled (Figure 5 and Figure S2). This is important because

as the correct topologies are sampled with higher accuracy, models start to reach the point where they can be subjected to atomic detail refinement to further increase their accuracy⁴⁶.

It is crucial to distinguish between the two major challenges in *de novo* structure prediction – sampling and scoring: The average improvement in sampling accuracy – i.e. the best model built among 5000 independent folding trajectories – of 0.8Å is moderate but significant. However, inclusion of the EPR data does not only allow folding of models that are more accurate, it greatly improves discrimination of incorrect models with a scoring function that combines BCL knowledge-based potentials and EPR restraints. Without using EPR restraints the average enrichment is 1.3, i.e. 13% of the most accurate models are in a sample of 10% best scoring models, which is close to chance. By using EPR data in addition to the knowledge-based score enrichment increases to 2.5, i.e. one out of four models in the 10% best scoring models also has the correct fold. This is important as it greatly improves the chance to identify correctly folded models, e.g. through clustering of good-scoring models. The combination of improved sampling and discrimination thereby significantly improves the reliability with which we were able to predict the tertiary structure of a protein.

The EPR distance data used for the present study is simulated from known experimental structures. It will be interesting to repeat this benchmark once sufficiently dense experimental datasets for several membrane proteins become available. For now, considerable effort was put forth to ensure that the simulated data mimics what would be obtained from a true EPR experiment, so that any results are unbiased by the simulated data. The previously published method for selecting distance restraints was used to create ten different datasets per protein³⁹. This ensures results are not biased by a particularly selected dataset. Previously, the uncertainty in the difference between spin label distances and the corresponding C_β distance ($D_{SL} - D_{BB}$) was

accounted for in simulated distance restraints by adding a random value between 12.5\AA and -2.5\AA ³⁹. Here, the probability of observing a given $D_{\text{SL}} - D_{\text{BB}}$ is used to determine the amount that should be added to the $C_{\beta} - C_{\beta}$ distance measured from the experimental structure.

Using a method developed for soluble proteins to select restraints for membrane proteins is not necessarily ideal. The constraints already imposed upon membrane proteins by the membrane geometry suggest that optimized methods for selecting restraints for membrane proteins should be developed. One such strategy could be to measure distances between transmembrane segments on the same side of the membrane, with the assumption that transmembrane helices are mostly rigid, parallel structures. Further, additional work is needed to account for topologically important SSEs that do not span the membrane, as well take into account the deviations of transmembrane segments from ideal geometries.

The improved sampling accuracy in the protein structure prediction process is primarily caused by the distance restraints. While by using EPR accessibility restraints the average μ_{10} over all twenty-nine proteins drops from 6.0\AA to 5.8\AA , by using EPR distance restraints μ_{10} can be improved to 5.1\AA .

Figure 5

Improved secondary structure predictions will improve the accuracy of predicted structures

The SSE pools are created in order to reduce the possibility of missing a SSE, which is generally a successful approach as demonstrated previously for soluble proteins³³. The helical transmembrane span prediction software Octopus⁴⁷ is used in conjunction with Jufo9D⁴⁸. Jufo9D

provides predictions for SSEs that do not necessarily span the membrane and therefore will not be predicted by Octopus. Improved secondary structure prediction methods will benefit membrane protein structure prediction. In addition, it has been demonstrated that the pattern of accessibility values for measurements along a sequence follow the periodicity of the SSE on which they are measured^{17,22,45}. Measured accessibility profiles could therefore be used to inform the pool of SSEs used for structure prediction.

The pool of SSEs used to assemble the membrane protein topologies is the most important determinant in successfully predicting the membrane proteins' structure. This is seen for 1U19 and 2BL2. With predicted SSEs, the structure of the two proteins can be sampled to a μ_{10} of 5.9Å and 6.2Å respectively (Table III). By using SSE definitions extracted from the experimentally determined structure, the proteins can be sampled at μ_{10} values of 4.4Å and 2.6Å. This is caused by secondary structure prediction methods breaking up transmembrane helices into several short helices making it harder to assemble the tertiary structure that does not have loop going through the membrane. The experiment was repeated with SSE definitions obtained from the experimentally determined structures of the proteins. While with predicted SSEs average μ_{10} , τ_4 and τ_8 values of 5.0Å, 6% and 19% are achieved over all twenty-nine proteins, by using the SSE definitions from the experimentally determined structure we could improve them to 4.5Å, 8% and 25%. In twenty-one out of twenty-nine cases the average accuracy of the ten best models by RMSD100 could be improved by using SSE definitions obtained from the experimentally determined structure (Figure 3). This shows that further improvements of the secondary structure prediction will also lead to an improved sampling accuracy of BCL::Fold.

Limitations of the cone model knowledge-based potential

The unknown label conformation is taken into account by the motion-on-a-cone model, which yields a $D_{SL} - D_{BB}$ distribution. This wide probability distribution accounts for two inherently different aspects – a structural and a dynamical: The structural effect looks at the relative position of the unpaired electron with respect to the protein backbone. This positioning is dependent on the protein structure, specifically the direction in which the $C_{\alpha} - C_{\beta}$ vector project into space with respect to the $C_{\alpha} - C_{\alpha}$ vector that links the two labeling site. As the cone model is applied in a model-independent fashion, it does not consider these geometric features but expresses the resulting ambiguity as part of the probability distribution. Second, chemical environment and exposure cause variable levels of spin label dynamics. These result in distance distributions of variable tightness in EPR experiments. This information is currently not considered as parameter in the cone model but absorbed by using a very wide $D_{SL} - D_{BB}$ probability distribution. This approach has the advantage that it is very robust with respect to uncertainties within the EPR experimental parameters and very fast to compute. At the same time, the cone model knowledge-based potential neglects important geometric parameters. Developing and testing approaches that take these parameters into account and lead to tighter distance distributions without losing the advantages of speed and robustness is an active area of our research.

Not considering geometrical features hinders the selection of accurate models for 1U19. EPR distance restraints improved the sampling accuracy, but it is still not possible to reliably select accurate models (Figure 4). While the distances observed in EPR experiments are typically long and therefore allow a broad range of topologically different models to fulfill them, inaccuracies in the translation from D_{SL} to D_{BB} also contribute to the selection problem. In the case of 1U19 the experimentally determined structure, which served as the template for the simulation of the

EPR distance restraints, shows a worse agreement with the restraints than the best scoring models. The spin-spin distance between residue 7 and residue 170 is 43.6Å while the distance between the C_{β} atoms is 35.7Å resulting in an agreement score of 0.3 on a scale from 0 to 1. By the EPR potential a C_{β} - C_{β} distance of 41.1Å is favorable which is accomplished by the sampled models with the best score leading to the selection of models, which deviate significantly, from the experimentally determined structure. Both spin-labeling sites are exposed, indicating they are at the outside of the protein. The projection angle between the C_{α} - C_{β} vectors is greater than 160° making it more likely that the spin labels are pointing away from each other. Those two properties allow the inference that we would expect are larger difference between D_{SL} and D_{BB} than 2.5Å. By using a knowledge- based potential, which also takes the exposure of the spin labeling sites and additional geometrical information into account a better ranking of the sampled models would be possible.

Ambiguities in the ranking of models remain

While the usage of restraints obtained from EPR experiments significantly improves the discrimination of incorrect models, ambiguities in the ranking of the models remain for multiple proteins in the benchmark set. This observation was especially pronounced for the proteins 1J4N, 1PV6, 1PY6, and 1U19 (Figure 5). In those cases, the best 10% of the models by BCL score cover a wide range of topologies. For 1PV6, the best 10% of the models by BCL score cover an RMSD100 range of 8Å when compared to the experimentally determined structure. Multiple factors are contributing to this observation. First, the BCL::Fold scoring function is an inaccurate approximation of free energy, which limits its discriminative power⁴². While adding a term that measures agreement with experimental data will improve its discriminative power, it appears that sparse restraints from EPR data are sometimes insufficient to remove all ambiguities. This is also

because, second, the translation of spin-label distance distributions into a backbone structural restraint introduces a substantial uncertainty and therefore allows sometimes multiple topologies to fulfill the restraint. One side effect of these approximations is that as shown in Figure 5 the native structure is not always in the global minimum of the BCL scoring function. Relaxing the experimentally determined protein structures in the BCL force field indicate that the closest minimum in the scoring function is between 1.5Å and 4.1Å in RMSD100 separate relative to the experimentally determined structures.

Conclusion

The determination of membrane protein folds from EPR distance and accessibility data is within reach if these restraints aid protein folding protocols such as BCL::MP-Fold. The ability of EPR data to improve the sampling of native-like topologies and the importance of EPR accessibility data for obtaining highest contact recovery values was demonstrated. Further, the EPR specific scores allow the selection of close-to-native models, thereby overcoming a major obstacle in *de novo* protein structure prediction. Refining EPR distance potentials to also take the exposure of the spin labelling sites as well as relative orientation of the C_{α} - C_{β} vector might provide a more accurate translation from spin-spin distance into backbone distance, thereby further increasing model quality.

Acknowledgements

We thank Cristian Altenbach and Wayne Hubbell for sharing their EPR data for rhodopsin with us and therefore enabling us to evaluate our algorithm based on experimentally determined data.

This research used resources of the Oak Ridge Leadership Computing Facility at the Oak Ridge National Laboratory, which is supported by the Office of Science of the U.S. Department of Energy under Contract No. DE-AC05-00OR22725.

Availability

The BCL software suite is available at <http://www.meilerlab.org/bclcommons> under academic and business site licenses. The BCL source code is published under the BCL license and is available at <http://www.meilerlab.org/bclcommons>.

References

1. Overington, J. P., Al-Lazikani, B. & Hopkins, A. L. How many drug targets are there? *Nat. Rev. Drug Discov.* **5**, 993–6 (2006).
2. Berman, H. M. *et al.* The Protein Data Bank. *Nucleic Acids Res.* **28**, 235–42 (2000).
3. Tusnády, G. E., Dosztányi, Z. & Simon, I. Transmembrane proteins in the Protein Data Bank: identification and classification. *Bioinformatics* **20**, 2964–72 (2004).
4. Bill, R. M. *et al.* Overcoming barriers to membrane protein structure determination. *Nat. Biotechnol.* **29**, 335–40 (2011).
5. Tate, C. G. & Schertler, G. F. X. Engineering G protein-coupled receptors to facilitate their structure determination. *Curr. Opin. Struct. Biol.* **19**, 386–95 (2009).
6. Tate, C. G. Practical Considerations of Membrane Protein Instability during Purification and Crystallisation. *Heterologous Expr. Membr. Proteins Methods Protoc.* **601**, 187–203 (2010).
7. Kobilka, B. K. G Protein Coupled Receptor Structure and Activation. *Biochim. Biophys. Acta* **1768**, 794–807 (2007).
8. Kang, C. & Li, Q. Solution NMR study of integral membrane proteins. *Curr. Opin. Chem. Biol.* **15**, 560–9 (2011).

9. Kim, H. J., Howell, S. C., Van Horn, W. D., Jeon, Y. H. & Sanders, C. R. Recent Advances in the Application of Solution NMR Spectroscopy to Multi-Span Integral Membrane Proteins. *Prog. Nucl. Magn. Reson. Spectrosc.* **55**, 335–360 (2009).
10. Alexander, N. S. *et al.* Energetic analysis of the rhodopsin-G-protein complex links the $\alpha 5$ helix to GDP release. *Nat. Struct. Mol. Biol.* **21**, 56–63 (2014).
11. Hubbell, W. L. & Altenbach, C. Investigation of structure and dynamics in membrane proteins using site-directed spin labeling. *Curr. Opin. Struct. Biol.* **4**, 566–573 (1994).
12. Dong, J., Yang, G. & Mchaourab, H. S. Structural basis of energy transduction in the transport cycle of MsbA. *Science* **308**, 1023–8 (2005).
13. Czogalla, A., Pieciul, A., Jezierski, A. & Sikorski, A. F. Attaching a spin to a protein -- site-directed spin labeling in structural biology. *Acta Biochim. Pol.* **54**, 235–44 (2007).
14. Koteiche, H. A., Berengian, A. R. & Mchaourab, H. S. Identification of protein folding patterns using site-directed spin labeling. Structural characterization of a β -sheet and putative substrate binding regions in the conserved domain of β A-crystallin. *Biochemistry* **37**, 12681–12688 (1998).
15. Koteiche, H. A. & Mchaourab, H. S. Folding pattern of the alpha-crystallin domain in alphaA-crystallin determined by site-directed spin labeling. *J. Mol. Biol.* **294**, 561–77 (1999).
16. Altenbach, C., Marti, T., Khorana, H. G. & Hubbell, W. L. Transmembrane protein structure: spin labeling of bacteriorhodopsin mutants. *Science* **248**, 1088–92 (1990).
17. Lietzow, M. a & Hubbell, W. L. Motion of spin label side chains in cellular retinol-binding protein: correlation with structure and nearest-neighbor interactions in an antiparallel beta-sheet. *Biochemistry* **43**, 3137–51 (2004).
18. Altenbach, C. *et al.* Structural features and light-dependent changes in the cytoplasmic interhelical E-F loop region of rhodopsin: a site-directed spin-labeling study. *Biochemistry* **35**, 12470–8 (1996).
19. Salwiński, L. & Hubbell, W. L. Structure in the channel forming domain of colicin E1 bound to membranes: the 402-424 sequence. *Protein Sci.* **8**, 562–72 (1999).
20. Borbat, P. P., Mchaourab, H. S. & Freed, J. H. Protein structure determination using long-distance constraints from double-quantum coherence ESR: study of T4 lysozyme. *J. Am. Chem. Soc.* **124**, 5304–14 (2002).
21. Jeschke, G. & Polyhach, Y. Distance measurements on spin-labelled biomacromolecules by pulsed electron paramagnetic resonance. *Phys. Chem. Chem. Phys.* **9**, 1895–910 (2007).

22. Zou, P., Bortolus, M. & Mchaourab, H. S. Conformational cycle of the ABC transporter MsbA in liposomes: detailed analysis using double electron-electron resonance spectroscopy. *J. Mol. Biol.* **393**, 586–97 (2009).
23. Altenbach, C., Kusnetzow, A. K., Ernst, O. P., Hofmann, K. P. & Hubbell, W. L. High-resolution distance mapping in rhodopsin reveals the pattern of helix movement due to activation. *Proc. Natl. Acad. Sci. U. S. A.* **105**, 7439–44 (2008).
24. Claxton, D. P. *et al.* Ion/substrate-dependent conformational dynamics of a bacterial homolog of neurotransmitter:sodium symporters. *Nat. Struct. Mol. Biol.* **17**, 822–9 (2010).
25. Chakrapani, S., Sompornpisut, P., Intharathep, P., Roux, B. & Perozo, E. The activated state of a sodium channel voltage sensor in a membrane environment. *Proc. Natl. Acad. Sci. U. S. A.* **107**, 5435–40 (2010).
26. Vásquez, V. *et al.* Three-dimensional architecture of membrane-embedded MscS in the closed conformation. *J. Mol. Biol.* **378**, 55–70 (2008).
27. Alexander, N. S., Bortolus, M., Al-Mestarihi, A., Mchaourab, H. S. & Meiler, J. De novo high-resolution protein structure determination from sparse spin-labeling EPR data. *Structure* **16**, 181–95 (2008).
28. Hirst, S. & Alexander, N. S. RosettaEPR: an integrated tool for protein structure determination from sparse EPR data. *J. Struct. Biol.* **173**, 506–514 (2011).
29. Vera, I. & Blackburn, M. Pulsed EPR Distance Measurements in Soluble Proteins by Site-Directed Spin Labeling (SDSL). *Curr. Protoc. Protein Sci.* 1–29 (2013). doi:10.1002/0471140864.ps1717s74
30. Yang, Y. *et al.* Combining NMR and EPR methods for homodimer protein structure determination. *J. Am. Chem. Soc.* **132**, 11910–3 (2010).
31. Yarov-Yarovoy, V., Schonbrun, J. & Baker, D. Multipass membrane protein structure prediction using Rosetta. *Proteins* **62**, 1010–25 (2006).
32. Barth, P., Wallner, B. & Baker, D. Prediction of membrane protein structures with complex topologies using limited constraints. *Proc. Natl. Acad. Sci. U. S. A.* **106**, 1409–14 (2009).
33. Karakaş, M. *et al.* BCL::Fold--de novo prediction of complex and large protein topologies by assembly of secondary structure elements. *PLoS One* **7**, e49240 (2012).
34. Weiner, B. E., Wötzel, N., Karakaş, M., Alexander, N. S. & Meiler, J. BCL::MP-fold: folding membrane proteins through assembly of transmembrane helices. *Structure* **21**, 1107–17 (2013).

35. Lindert, S. *et al.* EM-fold: De novo folding of alpha-helical proteins guided by intermediate-resolution electron microscopy density maps. *Structure* **17**, 990–1003 (2009).
36. Lindert, S. *et al.* EM-Fold: De Novo Atomic-Detail Protein Structure Determination from Medium-Resolution Density Maps. *Structure* **20**, 464–478 (2012).
37. Weiner, B. E. *et al.* BCL::Fold--protein topology determination from limited NMR restraints. *Proteins* **82**, 587–95 (2014).
38. Durham, E., Dorr, B., Wötzel, N., Staritzbichler, R. & Meiler, J. Solvent accessible surface area approximations for rapid and accurate protein structure prediction. *J. Mol. Model.* **15**, 1093–108 (2009).
39. Kazmier, K., Alexander, N. S., Meiler, J. & Mchaourab, H. S. Algorithm for selection of optimized EPR distance restraints for de novo protein structure determination. *J. Struct. Biol.* **173**, 549–57 (2011).
40. Eisenberg, D., Weiss, R. M. & Terwilliger, T. C. The hydrophobic moment detects periodicity in protein hydrophobicity. *Proc. Natl. Acad. Sci. U. S. A.* **81**, 140–4 (1984).
41. Chakrapani, S., Cuello, L. G., Cortes, D. M. & Perozo, E. Structural dynamics of an isolated voltage-sensor domain in a lipid bilayer. *Structure* **16**, 398–409 (2008).
42. Wötzel, N. *et al.* BCL::Score--knowledge based energy potentials for ranking protein models represented by idealized secondary structure elements. *PLoS One* **7**, e49242 (2012).
43. Carugo, O. & Pongor, S. A normalized root-mean-square distance for comparing protein three-dimensional structures. *Protein Sci.* 1470–1473 (2001). doi:10.1110/ps.690101.of
44. Dalmas, O. *et al.* Structural dynamics of the magnesium-bound conformation of CorA in a lipid bilayer. *Structure* **18**, 868–78 (2010).
45. Zou, P. & Mchaourab, H. S. Alternating access of the putative substrate-binding chamber in the ABC transporter MsbA. *J. Mol. Biol.* **393**, 574–85 (2009).
46. Barth, P., Schonbrun, J. & Baker, D. Toward high-resolution prediction and design of transmembrane helical protein structures. *Proc. Natl. Acad. Sci. U. S. A.* **104**, 15682–7 (2007).
47. Viklund, H. & Elofsson, A. OCTOPUS: improving topology prediction by two-track ANN-based preference scores and an extended topological grammar. *Bioinformatics* **24**, 1662–8 (2008).

48. Leman, J. K., Müller, R., Karakaş, M., Wötzel, N. & Meiler, J. Simultaneous prediction of protein secondary structure and transmembrane spans. *Proteins* **81**, 1127–40 (2013).

Figure legends

Translation from EPR data into structural restraints

Figure 1: EPR distance measurements measure distances between residues in a protein indirectly.

While the experiment determined the spin-spin distance (D_{SL}), a distance between the backbone atoms (D_{BB}) is needed during the *de novo* protein structure prediction process. Therefore, a translation from D_{SL} to D_{BB} is necessary. BCL::Fold uses a knowledge-based potential to evaluate the agreement of the distance between the C_{β} -atoms in the model with the experimentally determined spin-spin distances (B). EPR accessibility data is translated into structural restraints by summing up the hydrophobic moment vectors (C_{α} -atom to C_{β} -atom) of four consecutive residues (C). This is done twice: first the normalized C_{α} - C_{β} vectors are multiplied with the accessibility determined in the EPR experiment, the second time they are multiplied with the neighbor count of the residue in the model. The vectors are summed up for each approach and the projection angle between the two resulting vectors is scored, with an angle of 0° being the best and 180° being the worst agreement (D).

Structure prediction protocol

Figure 2: BCL::Fold assembles predicted secondary structure elements (SSEs) in the three-dimensional space to predict the tertiary structure of a protein. In a first step, the secondary structure is predicted using a consensus of several SSE prediction methods like Octopus and JUFO9D (A). Consequently, the predicted SSEs are added to the model and transformed using a Monte Carlo algorithm (B). The outcome of each transformation is evaluated with knowledge-

based potential functions scoring SSE packing, radius of gyration, amino acid exposure, and amino acid pairing, loop closure geometry, secondary structure length and content, SSE clashes and the agreement of the model with the provided EPR distance and accessibility restraints (C). Based on the difference in score between the model before and the model after applying the transformation the outcome is either accepted or rejected (D). This process is repeated until a specified number of iterations or a maximum number of steps without score improvement is reached. The resulting models are then ranked based on their score according to the knowledge-based potential functions (E).

Sampling accuracy, contact recovery, and enrichment results

Figure 3: By using EPR distance and accessibility data in the structure prediction process, the sampling accuracy can be improved significantly for monomeric (circles) as well as oligomeric (squares) proteins (A). The sampling accuracy could be improved in twenty-five out of twenty-nine cases by using EPR distance and accessibility data, which is shown in by comparing the average RMSD100 values of the 1% most accurate models predicted without (x-axis) and with EPR data (y-axis) in (A). Adding protein specific structural information in the form of EPR distance and accessibility restraints also improves our ability to select the most accurate models among the sample ones. In each of the twenty-nine cases, EPR distance and accessibility restraints enable us to select more accurate models when compared to structure prediction without EPR data available. Shown are the average (line) and best (dot/square) RMSD100 values of the best 1% models by BCL score with (y-axis) and without (x-axis) EPR restraints (B). By using EPR accessibility data only (y-axis) the Contact Recovery could be improved in twenty-two out of twenty-nine cases (C) when compared to structure prediction without EPR accessibility restraints (x-axis). Improvements in secondary structure element (SSE) prediction

methods would also lead to improved sampling accuracies (D, see also Table S1). In twenty-one out of twenty-nine cases the average RMSD100 of the ten most accurate models could be improved by using SSE definitions obtained from the experimentally determined structure (y-axis) compared to using a predicted SSEs.

Limitations of the CONE model

Figure 4: For 1U19, the most accurate model cannot be reliably selected (A). One reason for that is, that the translation from the observed spin-spin distance to the backbone distance is inaccurate resulting in models which deviate topologically from the experimentally determined structure achieving a better agreement with the EPR distance restraints than the experimentally determined structure (B, two SSEs were removed to improve readability). This is demonstrated by the plot showing the correlation between the agreement with the EPR distance restraints (y-axis) and the RMSD100 relative to the experimentally determined structure (x-axis). The EPR potential does not take the exposure of the spin labelling site and the orientation of the $C_{\alpha}C_{\beta}$ vectors into account leading to inaccuracies when translating D_{SL} into D_{BB} for the residues 7 and 170 of 1U19. Both spin labels are at the outside of the protein and on different sides of the structure leading to greater difference between D_{SL} and D_{BB} .

Gallery of the structure prediction results

Figure 5: By using EPR distance and accessibility restraints, the sampling accuracy is significantly improved as the selection ability regarding accurate models. For selected proteins a comparison of the RMSD100 (column A) and Contact Recovery (column B) distributions for sampling with (red) and without (black) EPR restraints is shown. The y-axis of column A shows the cumulative density of models with respect to the RMSD100. The y-axis of column B shows

the cumulative density of models with respect to their contact recovery. Column C shows the correlation between the BCL score and the RMSD100 for the models sampled with EPR restraints (black dots) and the experimentally determined structure (red dot). The y-axis is the pseudo-energy score the algorithm assigned to the structure; the x-axis is the RMSD100 relative to the experimentally determined structure. The superimpositions show the best models by RMSD100 for folding with EPR restraints (column D), the best model by pseudo-energy score for folding with EPR restraints (column E), and the best model by pseudo-energy score for folding without EPR restraints (column F) superimposed with the experimentally determined structure (grey).

Table legends

The proteins used for benchmarking the algorithm

Table I: The twenty-nine proteins for the benchmark were chosen to cover a wide range of sequence length, number of secondary structure elements (SSEs) as well as number and percentage of residues within SSEs while having a mutual sequence identity of less than 20%. The columns denote the sequence length, the number of SSEs, the number of residues within SSEs, and the percentage of the residues is within SSEs. The proteins above the separating line are monomeric proteins; below the separating line are multimeric proteins. 2HAC, 2ZY9, and 3CAP are homo-dimers, 2BHW and 2H8A are homo-trimers, and 2L35 is a hetero-dimer. 1GZM was additionally included for the usage of experimentally determined data.

Enrichments achieved for folding with and without EPR restraints

Table II: EPR restraints significantly improve our ability to select the most accurate models among the sampled ones. When using EPR distance and accessibility restraints the enrichment

(E_{EPR}) could be improved in each case compared to structure prediction without EPR data (E_{None}). To be independent from specific spin labeling patterns ten different EPR distance restraint sets were used and the standard deviation regarding enrichment computed (σ_{EPR}). The experiment was also conducted using accessibility (E_{Acc}) and distance restraints (E_{Dist} and σ_{Dist}) only. In addition to using predicted secondary structure elements (Predicted Pool), the experiment was repeated using secondary structure elements obtained from the experimentally determined structure (Native Pool).

Sampling accuracy comparison for folding with and without EPR restraints

Table III: Results for folding the proteins based on predicted secondary structure elements without restraints, with accessibility restraints only, with distance restraints only and with accessibility and distance restraints. Shown are the RMSD100 of the most accurate model sampled (best), the average RMSD100 of the ten most accurate models (μ_{10}) as well as the percentage of the sampled models with RMSD100 values of less than 4Å and 8Å (τ_4 and τ_8). Using protein specific data derived from EPR experiments significantly improves the sampling accuracy. The improvement is mainly caused by using EPR distance restraints; accessibility restraints have a minor effect on the sampling accuracy.

Contact recovery comparison for folding with and without EPR restraints

Table IV: The usage of EPR accessibility restraints significantly increases the percentage of recovered contacts (amino acids that are separated by at least six residues and have a maximum Euclidean distance of 8Å in the experimentally determined structure). Shown are the highest contact recovery achieved (best), the average contact recovery of the ten models with the highest contact recovery (φ_{10}) and the percentage of models for which more than 20% and 40% of the contacts were recovered (γ_{20}, γ_{40}).

Table I

PDBID	length	# SSE	# res _{SSE}	% res _{SSE}	source	resolution[Å]
1IWG	168	5	152	90	X-Ray (PDB)	3.5
1GZM	349	7	216	62	X-Ray (PDB)	2.7
1J4N	116	4	93	80	X-Ray (PDB)	2.2
1KPL	203	8	155	76	X-Ray (PDB)	3.0
1OCC	191	5	142	74	X-Ray (PDB)	2.8
1OKC	297	9	211	71	X-Ray (PDB)	2.2
1PV6	189	8	165	87	X-Ray (PDB)	3.5
1PY6	227	9	171	75	X-Ray (PDB)	1.8
1RHZ	166	5	108	65	X-Ray (PDB)	3.5
1U19	278	7	183	66	X-Ray (PDB)	2.2
1XME	568	18	439	79	X-Ray (PDB)	2.3
2BG9	91	3	79	87	EM (PDB)	
2BL2	145	4	127	88	X-Ray (PDB)	2.1
2BS2	217	8	174	80	X-Ray (PDB)	1.8
2IC8	182	7	123	68	X-Ray (PDB)	2.1
2K73	164	5	102	62	NMR (PDB)	
2KSF	107	4	69	64	NMR (PDB)	
2KSY	223	7	174	78	NMR (PDB)	
2NR9	196	8	147	75	X-Ray (PDB)	2.2
2XUT	524	16	377	72	X-Ray (PDB)	3.6
3GIA	433	15	352	81	X-Ray (PDB)	2.2
3KCU	285	10	190	67	X-Ray (PDB)	2.2
3KJ6	366	8	171	47	X-Ray (PDB)	3.4
3P5N	189	6	132	70	X-Ray (PDB)	3.6
2BHW	669	12	303	45	X-Ray (PDB)	2.5
2H8A	363	12	285	79	EM (PDB)	3.2
2HAC	66	2	52	79	NMR	
2L35	95	3	77	81	NMR (PDB)	
2ZY9	344	16	310	90	X-Ray (PDB)	2.9
3CAP	696	18	474	68	NMR	2.9

Table II

Target	Predicted Pool						Native Pool					
	E_{None}	E_{Acc}	E_{Dist}	σ_{Dist}	E_{EPR}	σ_{EPR}	E_{None}	E_{Acc}	E_{Dist}	σ_{Dist}	E_{EPR}	σ_{EPR}
1IWG	1.1	1.5	2.2	0.2	2.3	0.2	0.4	0.9	1.2	0.4	2.2	0.3
1J4N	0.4	0.3	1.7	0.2	1.8	0.2	0.5	0.6	0.9	0.2	1.7	0.3
1KPL	2.2	2.4	2.4	0.1	2.4	0.3	0.3	0.3	2.4	0.4	2.4	0.2
1OCC	1.5	1.5	4.0	1.0	5.1	1.0	1.8	1.8	3.9	1.0	5.0	1.0
1OKC	1.3	1.4	1.7	0.2	1.7	0.2	1.3	1.4	1.5	0.1	1.7	0.2
1PV6	1.2	1.3	1.9	0.2	1.9	0.3	0.5	1.0	1.7	0.4	2.0	0.3
1PY6	2.1	2.0	3.2	0.3	3.3	0.3	2.3	2.3	3.2	0.3	3.3	0.3
1RHZ	1.1	1.3	1.8	0.4	2.1	0.6	1.3	1.4	1.6	0.4	1.4	0.7
1U19	1.6	2.2	2.6	0.2	2.6	0.2	2.0	1.7	2.0	0.3	2.9	0.7
1XME	1.4	1.3	1.7	0.3	1.7	0.3	1.1	1.0	1.7	0.3	3.6	0.5
2BG9	0.9	1.8	2.5	0.5	2.5	0.4	1.6	2.7	1.6	0.6	1.9	0.8
2BL2	0.5	0.5	1.4	0.3	1.4	0.3	1.1	0.7	3.1	0.5	4.9	1.0
2BS2	2.0	2.0	2.6	0.2	2.6	0.1	1.9	2.3	2.4	0.3	2.8	0.3
2IC8	1.0	1.2	1.6	0.3	1.7	0.2	1.2	1.2	1.7	0.3	2.8	0.7
2K73	2.1	1.5	1.6	0.6	2.1	0.2	2.2	2.4	2.8	0.6	7.8	0.7
2KSF	2.6	2.5	2.4	0.8	2.6	0.7	3.8	3.2	2.1	0.7	2.3	0.7
2KSY	1.7	2.2	2.6	0.7	3.0	0.6	2.3	2.0	3.3	0.6	3.8	1.1
2NR9	0.8	0.9	1.0	0.2	1.1	0.2	1.6	1.2	1.5	0.3	1.9	0.2
2XUT	1.2	1.3	1.6	0.2	1.6	0.2	0.5	0.5	1.3	0.2	2.1	0.3
3GIA	0.7	0.7	1.2	0.2	1.2	0.2	0.5	0.6	0.8	0.2	0.5	0.1
3KCU	0.8	1.5	1.6	0.2	1.7	0.2	1.3	1.1	1.6	0.2	1.8	0.5
3KJ6	1.6	2.0	2.3	0.2	2.2	0.2	1.4	1.7	2.0	0.3	4.2	0.8
3P5N	0.8	1.3	1.5	0.3	1.6	0.3	1.3	1.1	1.7	0.3	2.3	0.8
2BHW	0.8	0.9	2.1	0.6	2.3	0.5	1.2	1.7	3.9	1.2	4.4	1.7
2H8A	2.1	2.4	6.3	0.4	6.2	0.7	1.6	2.1	5.8	0.9	7.2	0.9
2HAC	0.8	2.8	3.4	0.6	4.0	0.9	0.5	2.4	1.2	0.2	2.5	0.7
2L35	0.8	1.7	1.9	0.7	1.9	0.7	0.8	1.0	2.3	0.9	2.6	1.2
2ZY9	0.7	2.3	2.4	0.2	2.9	0.3	1.0	1.4	2.0	0.4	3.1	0.4
3CAP	1.3	1.8	3.3	0.4	3.7	0.4	1.7	2.2	3.1	0.8	3.8	0.2
∅	1.3	1.6	2.3	0.3	2.5	0.4	1.4	1.5	2.2	0.5	3.1	0.6

Table III

Target	None				Accessibility				Distance				Distance + Accessibility			
	best	μ_{10}	T_4	T_8	best	μ_{10}	T_4	T_8	best	μ_{10}	T_4	T_8	best	μ_{10}	T_4	T_8
1IWG	4.2	4.9	0.0	19.1	3.9	4.3	0.1	26.3	3.8	4.4	0.0	22.1	3.6	4.2	0.1	25.8
1J4N	5.2	5.3	0.0	18.0	4.2	4.7	0.0	22.5	4.4	4.8	0.0	21.0	3.8	4.3	0.0	25.4
1KPL	10.1	10.3	0.0	0.0	8.8	9.6	0.0	0.0	8.5	9.4	0.0	0.0	8.5	9.3	0.0	0.0
1OCC	3.7	4.5	0.0	20.1	2.2	2.9	0.8	30.2	2.4	2.8	3.1	44.9	2.0	2.3	7.0	50.8
1OKC	6.4	6.8	0.0	1.2	8.2	8.8	0.0	0.0	7.1	7.8	0.0	0.1	6.9	7.7	0.0	0.2
1PV6	5.2	6.1	0.0	5.3	5.3	5.8	0.0	6.0	5.2	5.7	0.0	8.5	4.9	5.5	0.0	10.5
1PY6	4.4	5.1	0.0	15.2	3.9	4.3	0.0	17.5	3.6	4.2	0.1	24.2	3.3	3.8	0.2	26.7
1RHZ	5.6	5.9	0.0	2.1	5.5	5.7	0.0	1.9	4.2	4.7	0.0	5.6	3.9	4.4	0.0	7.0
1U19	5.3	5.7	0.0	4.7	5.4	6.1	0.0	3.0	5.5	6.2	0.0	3.6	5.2	5.9	0.0	4.1
1XME	8.0	8.7	0.0	0.0	8.1	8.7	0.0	0.0	7.3	7.8	0.0	0.2	7.2	7.8	0.0	0.2
2BG9	2.3	2.6	10.8	52.7	2.2	2.3	28.1	51.3	2.2	2.3	28.1	57.7	2.1	2.2	32.6	61.3
2BL2	7.5	8.4	0.0	0.0	7.8	8.4	0.0	0.0	5.0	6.1	0.0	0.9	5.1	6.2	0.0	0.8
2BS2	6.1	6.3	0.0	2.4	6.3	6.6	0.0	1.8	5.3	5.9	0.0	3.5	5.2	5.8	0.0	3.5
2IC8	5.5	6.1	0.0	4.7	6.0	6.2	0.0	4.2	5.0	5.5	0.0	9.8	5.1	5.5	0.0	9.4
2K73	3.3	3.6	0.5	24.8	3.3	3.5	0.7	21.4	2.7	3.0	3.4	30.1	2.8	3.1	3.3	30.0
2KSF	4.1	4.4	0.0	22.3	2.6	3.0	2.6	21.9	2.9	3.1	5.2	25.9	2.7	2.9	8.3	25.1
2KSY	4.9	5.3	0.0	11.2	3.7	4.5	0.0	13.4	3.5	4.1	0.1	21.4	3.6	4.1	0.1	20.4
2NR9	5.6	6.0	0.0	5.8	6.0	6.6	0.0	3.4	6.4	6.9	0.0	2.5	6.4	6.9	0.0	2.5
2XUT	7.7	8.5	0.0	0.0	7.5	8.4	0.0	0.0	7.7	8.2	0.0	0.1	7.7	8.2	0.0	0.1
3GIA	10.0	10.2	0.0	0.0	9.5	9.8	0.0	0.0	9.1	9.6	0.0	0.0	9.1	9.6	0.0	0.0
3KCU	7.0	7.5	0.0	0.3	7.7	8.1	0.0	0.0	6.3	7.2	0.0	0.6	6.5	7.3	0.0	0.4
3KJ6	6.6	7.0	0.0	0.7	4.9	6.4	0.0	1.0	5.2	5.9	0.0	3.0	4.9	5.8	0.0	3.0
3P5N	4.6	5.8	0.0	5.5	5.3	5.8	0.0	4.5	4.8	5.6	0.0	10.2	4.8	5.6	0.0	10.0
2BHW	7.4	7.8	0.0	0.2	6.9	7.4	0.0	0.3	3.0	3.4	0.9	31.7	2.9	3.4	0.9	31.2
2H8A	3.3	3.9	0.1	32.5	3.1	3.8	0.2	34.5	1.9	2.1	6.4	41.7	1.8	2.0	7.6	44.3
2HAC	1.3	1.4	75.3	89.6	1.3	1.4	83.7	94.8	1.3	1.5	71.8	92.1	1.3	1.5	87.0	96.8
2L35	2.6	2.9	4.5	19.8	1.7	1.8	17.1	22.4	1.9	2.1	31.0	48.3	1.9	2.1	31.0	48.3
2ZY9	4.7	5.7	0.0	3.4	4.5	5.5	0.0	4.4	2.7	3.3	0.4	21.4	2.8	3.4	0.3	20.9
3CAP	7.4	8.0	0.0	0.1	7.3	7.9	0.0	0.1	4.9	5.4	0.0	5.8	4.7	5.3	0.0	4.1
∅	5.5	6.0	3.0	12.5	5.3	5.8	4.6	13.3	4.6	5.1	5.2	18.0	4.5	5.0	6.2	19.4

Table IV

Target	None				Accessibility				Distance				Distance + Accessibility			
	best	Φ_{10}	Υ_{20}	Υ_{40}	best	Φ_{10}	Υ_{20}	Υ_{40}	best	Φ_{10}	Υ_{20}	Υ_{40}	best	Φ_{10}	Υ_{20}	Υ_{40}
1IWG	23.7	21.3	0.2	0.0	33.5	29.4	2.0	0.0	31.3	26.9	1.2	0.0	33.8	28.3	2.9	0.0
1J4N	31.6	28.7	2.7	0.0	45.9	39.7	13.5	0.1	40.5	36.8	11.2	0.0	44.8	39.8	22.5	0.3
1KPL	22.8	14.4	0.0	0.0	18.7	15.5	0.0	0.0	19.0	15.6	0.0	0.0	18.4	16.1	0.0	0.0
1OCC	44.0	34.3	1.7	0.0	77.1	57.8	20.7	1.1	63.0	55.9	15.4	1.5	66.1	59.4	25.6	4.6
1OKC	15.4	11.0	0.0	0.0	22.0	16.4	0.0	0.0	19.5	16.4	0.0	0.0	19.8	17.6	0.0	0.0
1PV6	19.6	13.9	0.0	0.0	23.6	20.6	0.1	0.0	22.1	19.0	0.1	0.0	22.7	19.5	0.1	0.0
1PY6	21.0	19.1	0.0	0.0	35.1	30.4	2.2	0.0	32.8	27.4	1.4	0.0	36.0	31.1	3.5	0.0
1RHZ	33.0	29.2	1.6	0.0	38.1	35.1	6.2	0.0	41.9	36.0	7.0	0.1	41.8	37.2	11.3	0.2
1U19	25.4	17.3	0.0	0.0	25.8	22.7	0.2	0.0	21.9	18.4	0.0	0.0	23.8	19.0	0.1	0.0
1XME	10.0	8.5	0.0	0.0	10.6	9.2	0.0	0.0	9.6	8.3	0.0	0.0	10.1	8.8	0.0	0.0
2BG9	79.5	73.9	37.5	5.4	95.5	90.9	93.0	52.2	84.1	78.2	51.2	16.5	92.5	87.8	78.3	40.6
2BL2	18.3	14.8	0.0	0.0	25.7	20.9	0.1	0.0	31.7	23.9	0.2	0.0	28.7	23.0	0.3	0.0
2BS2	23.9	21.7	0.3	0.0	32.5	28.9	1.0	0.0	27.6	24.8	0.4	0.0	34.2	28.8	1.2	0.0
2IC8	27.4	21.8	0.2	0.0	29.9	26.2	1.0	0.0	26.2	23.4	0.3	0.0	34.5	29.0	2.1	0.0
2K73	44.2	39.8	6.5	0.1	65.1	60.3	37.2	3.7	52.3	47.8	14.0	0.5	65.8	60.7	38.5	6.7
2KSF	47.2	37.0	4.1	0.0	73.6	66.6	28.6	3.4	58.5	53.0	16.6	0.8	71.5	65.2	35.9	6.6
2KSY	29.6	22.2	0.2	0.0	37.6	31.5	3.3	0.0	38.8	28.9	1.4	0.0	37.7	31.5	2.9	0.0
2NR9	24.1	20.0	0.1	0.0	27.4	22.7	0.4	0.0	25.1	20.9	0.1	0.0	24.4	23.4	0.3	0.0
2XUT	9.8	9.0	0.0	0.0	12.3	10.0	0.0	0.0	10.0	9.7	0.0	0.0	10.1	8.9	0.0	0.0
3GIA	7.6	6.5	0.0	0.0	8.3	7.0	0.0	0.0	7.6	6.8	0.0	0.0	7.8	6.5	0.0	0.0
3KCU	19.1	15.5	0.0	0.0	21.5	18.4	0.0	0.0	21.2	17.6	0.0	0.0	20.3	19.0	0.0	0.0
3KJ6	18.4	15.9	0.0	0.0	29.5	22.1	0.1	0.0	21.7	19.6	0.1	0.0	25.4	21.8	0.2	0.0
3P5N	29.8	21.2	0.1	0.0	33.0	29.2	1.2	0.0	30.9	25.3	0.2	0.0	30.9	30.0	0.9	0.0
2BHW	42.2	36.8	2.3	0.0	46.8	40.0	3.8	0.2	49.5	43.1	4.2	0.2	48.9	42.3	4.4	0.2
2H8A	28.8	19.5	0.0	0.0	30.9	28.2	1.1	0.0	44.8	40.9	7.2	0.2	49.8	45.7	10.7	0.7
2HAC	100.0	98.9	87.0	80.4	100.0	98.0	90.9	83.1	99.4	98.0	81.7	73.1	99.4	97.7	82.6	75.2
2L35	53.2	49.2	11.1	0.5	76.6	73.8	53.2	15.2	49.4	47.3	26.6	0.9	76.0	70.6	79.0	18.9
2ZY9	16.9	14.2	0.0	0.0	27.1	23.7	0.3	0.0	29.6	24.7	0.3	0.0	36.8	30.9	1.4	0.0
3CAP	12.7	11.9	0.0	0.0	17.9	14.0	0.0	0.0	14.4	12.3	0.0	0.0	17.5	14.2	2.8	0.0
∅	30.3	25.8	5.4	3.0	38.7	34.1	12.4	5.5	35.3	31.3	8.3	3.2	38.9	35.0	14.1	5.3

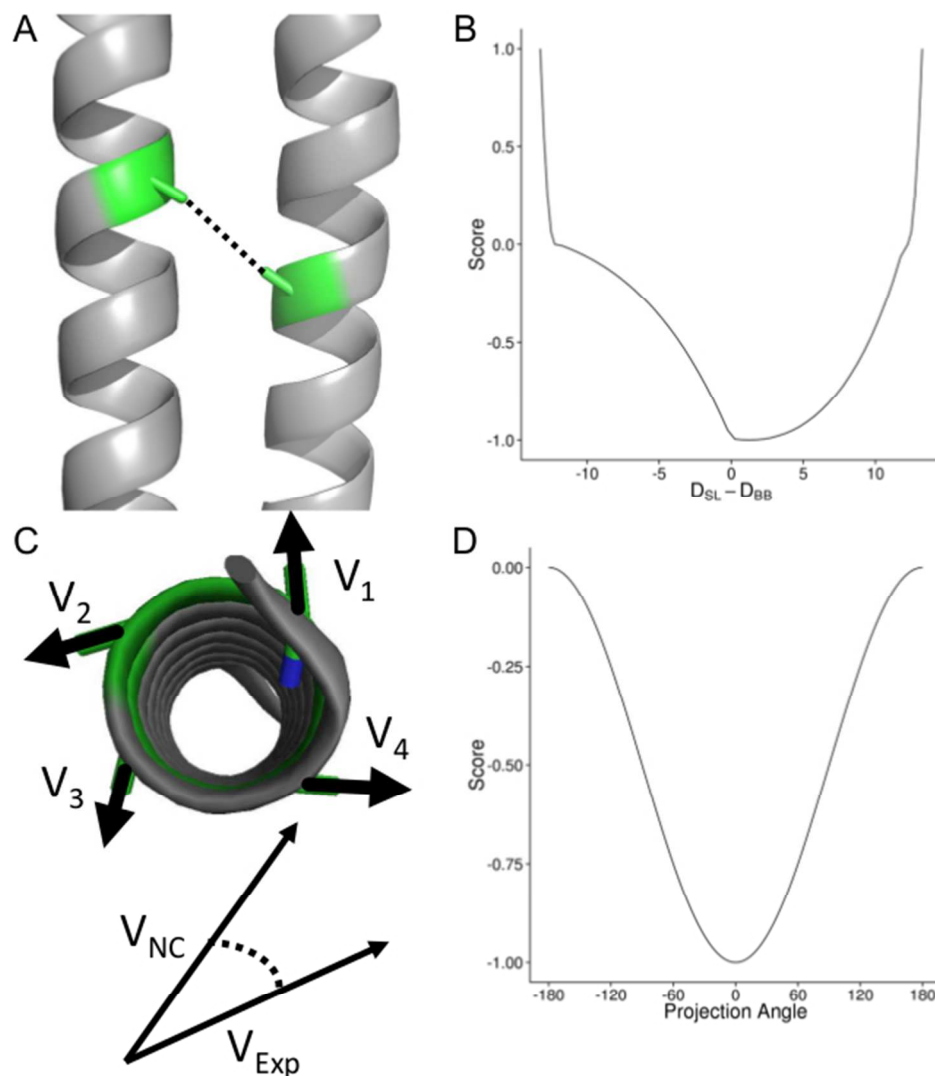


Figure 1

EPR distance measurements measure distances between residues in a protein indirectly. While the experiment determined the spin-spin distance (DSL), a distance between the backbone atoms (DBB) is needed during the de novo protein structure prediction process. Therefore, a translation from DSL to DBB is necessary. BCL::Fold uses a knowledge-based potential to evaluate the agreement of the distance between the $C\beta$ -atoms in the model with the experimentally determined spin-spin distances (B). EPR accessibility data is translated into structural restraints by summing up the hydrophobic moment vectors (Ca-atom to $C\beta$ -atom) of four consecutive residues (C). This is done twice: first the normalized Ca - $C\beta$ vectors are multiplied with the accessibility determined in the EPR experiment, the second time they are multiplied with the neighbor count of the residue in the model. The vectors are summed up for each approach and the projection angle between the two resulting vectors is scored, with an angle of 0° being the best and 180° being the worst agreement (D).

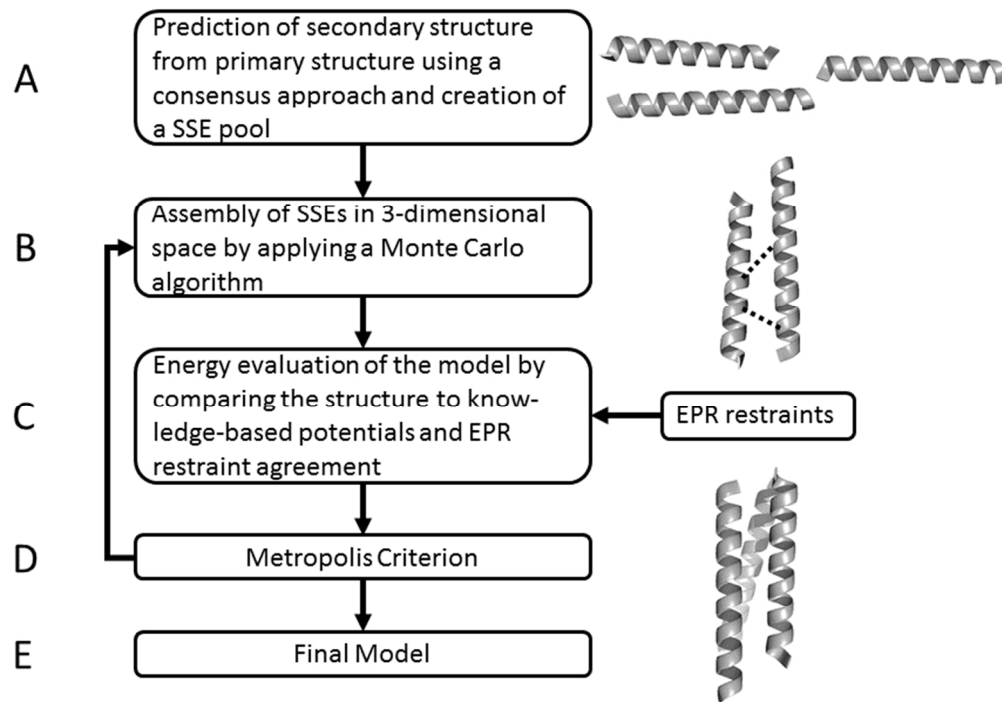


Figure 2

BCL::Fold assembles predicted secondary structure elements (SSEs) in the three-dimensional space to predict the tertiary structure of a protein. In a first step, the secondary structure is predicted using a consensus of several SSE prediction methods like Octopus and JUF09D (A). Consequently, the predicted SSEs are added to the model and transformed using a Monte Carlo algorithm (B). The outcome of each transformation is evaluated with knowledge-based potential functions scoring SSE packing, radius of gyration, amino acid exposure, and amino acid pairing, loop closure geometry, secondary structure length and content, SSE clashes and the agreement of the model with the provided EPR distance and accessibility restraints (C). Based on the difference in score between the model before and the model after applying the transformation the outcome is either accepted or rejected (D). This process is repeated until a specified number of iterations or a maximum number of steps without score improvement is reached. The resulting models are then ranked based on their score according to the knowledge-based potential functions (E).

Acce

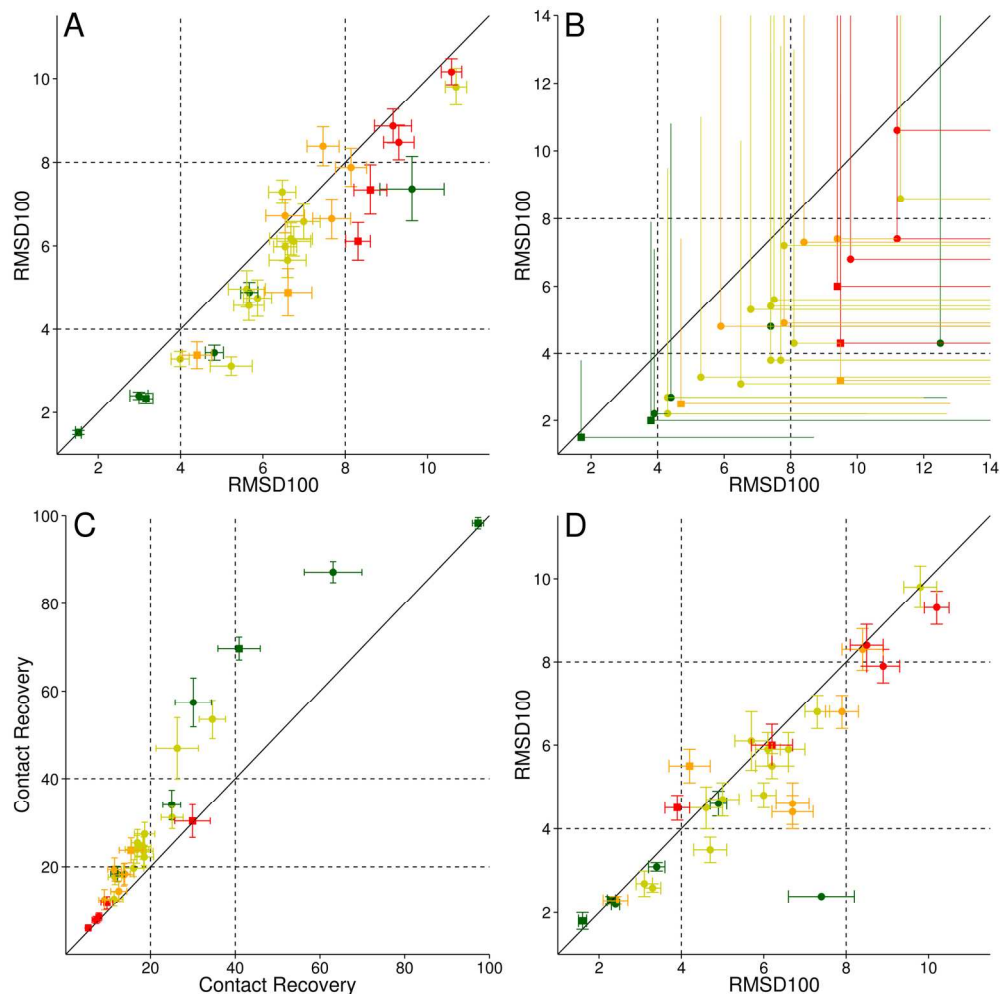


Figure 3

By using EPR distance and accessibility data in the structure prediction process, the sampling accuracy can be improved significantly for monomeric (circles) as well as oligomeric (squares) proteins (A). The sampling accuracy could be improved in twenty-five out of twenty-nine cases by using EPR distance and accessibility data, which is shown in by comparing the average RMSD100 values of the 1% most accurate models predicted without (x-axis) and with EPR data (y-axis) in (A). Adding protein specific structural information in the form of EPR distance and accessibility restraints also improves our ability to select the most accurate models among the sample ones. In each of the twenty-nine cases, EPR distance and accessibility restraints enable us to select more accurate models when compared to structure prediction without EPR data available. Shown are the average (line) and best (dot/square) RMSD100 values of the best 1% models by BCL score with (y-axis) and without (x-axis) EPR restraints (B). By using EPR accessibility data only (y-axis) the Contact Recovery could be improved in twenty-two out of twenty-nine cases (C) when compared to structure prediction without EPR accessibility restraints (x-axis). Improvements in secondary structure element (SSE) prediction methods would also lead to improved sampling accuracies (D, see also Table S1).

In twenty-one out of twenty-nine cases the average RMSD100 of the ten most accurate models could be improved by using SSE definitions obtained from the experimentally determined structure (y-axis) compared to using a predicted SSEs.

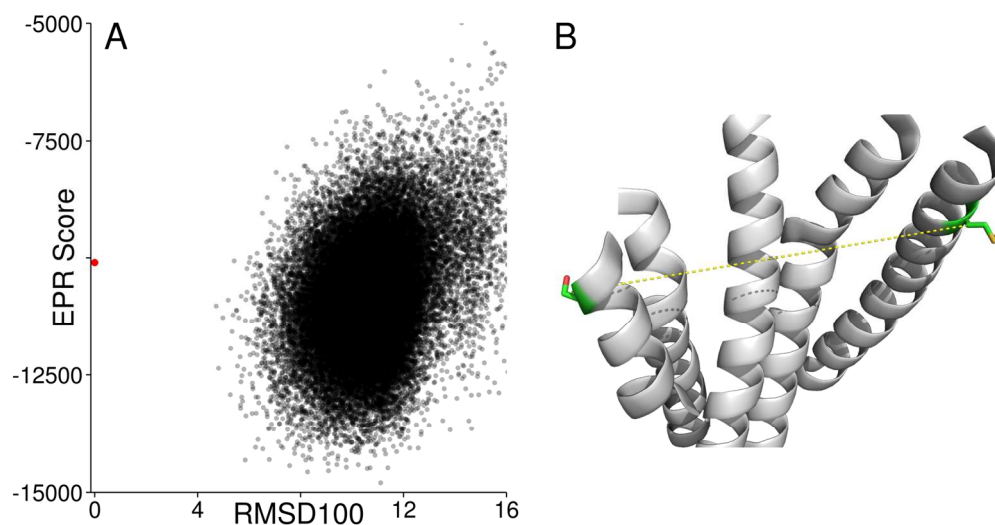


Figure 4

For 1U19, the most accurate model cannot be reliably selected (A). One reason for that is, that the translation from the observed spin-spin distance to the backbone distance is inaccurate resulting in models which deviate topologically from the experimentally determined structure achieving a better agreement with the EPR distance restraints than the experimentally determined structure (B, two SSEs were removed to improve readability). This is demonstrated by the plot showing the correlation between the agreement with the EPR distance restraints (y-axis) and the RMSD100 relative to the experimentally determined structure (x-axis). The EPR potential does not take the exposure of the spin labelling site and the orientation of the C α C β vectors into account leading to inaccuracies when translating DSL into DBB for the residues 7 and 170 of 1U19. Both spin labels are at the outside of the protein and on different sides of the structure leading to greater difference between DSL and DBB.

Accept

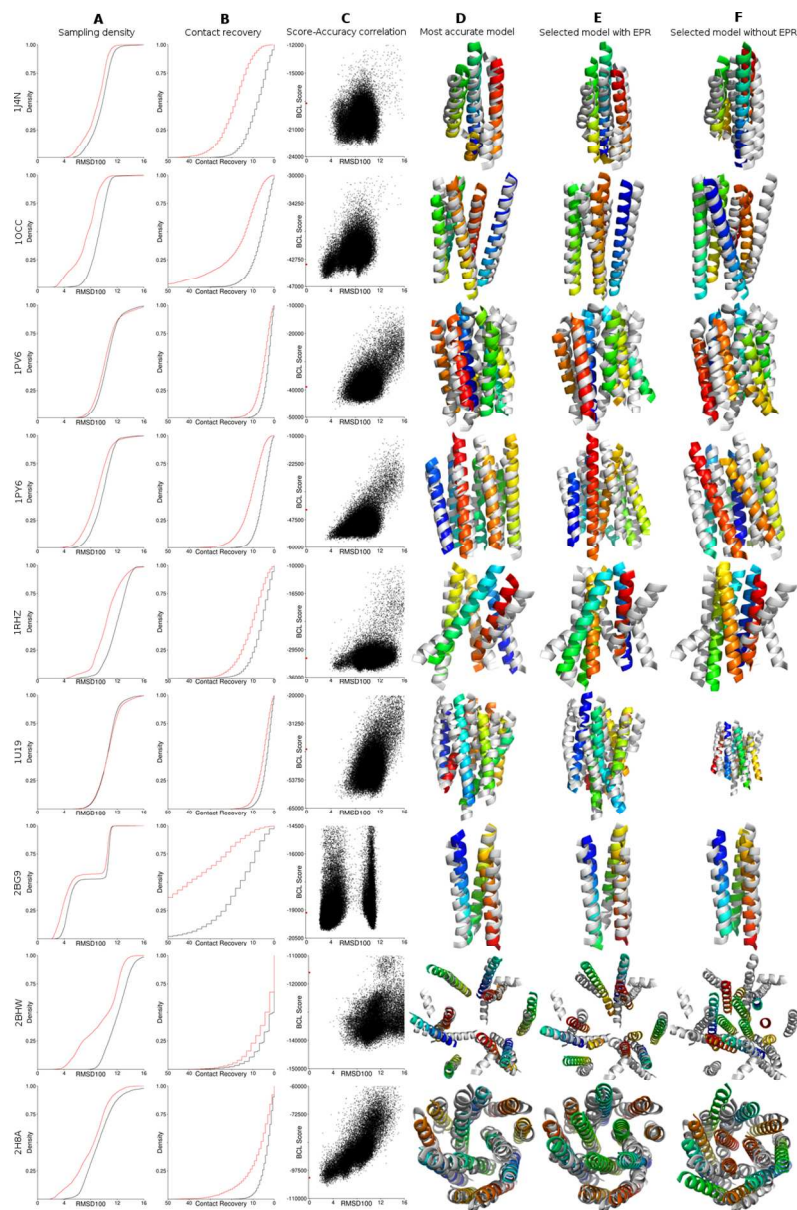


Figure 5

By using EPR distance and accessibility restraints, the sampling accuracy is significantly improved as the selection ability regarding accurate models. For selected proteins a comparison of the RMSD100 (column A) and Contact Recovery (column B) distributions for sampling with (red) and without (black) EPR restraints is shown. The y-axis of column A shows the cumulative density of models with respect to the RMSD100. The y-axis of column B shows the cumulative density of models with respect to their contact recovery. Column C shows the correlation between the BCL score and the RMSD100 for the models sampled with EPR restraints (black dots) and the experimentally determined structure (red dot). The y-axis is the pseudo-energy score the algorithm assigned to the structure; the x-axis is the RMSD100 relative to the experimentally determined structure. The superimpositions show the best models by RMSD100 for folding with EPR restraints (column D), the best model by pseudo-energy score for folding with EPR restraints (column E), and the best model by pseudo-energy score for folding without EPR restraints (column F) superimposed with the experimentally determined structure (grey).